

Compressibility trends of the clinopyroxenes, and in-situ high-pressure single-crystal X-ray diffraction study of jadeite

ANDREW C. MCCARTHY,* ROBERT T. DOWNS, AND RICHARD M. THOMPSON

Department of Geosciences, University of Arizona, Tucson, Arizona 85721-0077, U.S.A.

ABSTRACT

The crystal structure of a natural jadeite, NaAlSi₂O₆, was studied at room temperature over the pressure range 0–9.17 GPa using single-crystal X-ray diffraction. Unit-cell data were determined at 16 pressures, and intensity data were collected at nine of these pressures. A third-order Birch-Murnaghan equation of state fit to the *P-V* data yielded $V_0 = 402.03(2) \text{ \AA}^3$, $K_0 = 136.5(14) \text{ GPa}$, and $K'_0 = 3.4(4)$. Jadeite exhibits strongly anisotropic compression with unit strain axial ratios of 1.00:1.63:2.10. Silicate chains become more O-rotated with pressure, reducing $\angle O3-O3-O3$ from $174.7(1)^\circ$ at ambient pressure to $169.2(6)^\circ$ at 9.17 GPa and bringing the anions of jadeite closer to a cubic closest-packed arrangement. No evidence of a phase transition was observed over the studied pressure range.

In an effort to understand pyroxene compressibilities, selected clinopyroxene bulk moduli were plotted against ambient unit-cell volumes. Two trends were identified and are explained in terms of differences in M2-O3 bonding topologies and the geometric relationship of the bonds with tetrahedral rotation in the silicate chains. Bonds positioned to favor the tetrahedral rotation upon compression are termed “sympathetic,” whereas bonds positioned to resist the rotation are termed “antipathetic.” Examination of the different pyroxene structures indicates that structures containing antipathetic M2-O3 bonds are less compressible than those with only sympathetic M2-O3 bonds. This behavior has not been previously recognized.

Keywords: Jadeite, crystal structure, high pressure, single-crystal X-ray diffraction, pyroxene, clinopyroxene, compressibility, elasticity, bulk modulus

INTRODUCTION

This study examines the compressibilities of *C2/c* and *P2₁/c* clinopyroxenes, taken from the literature, in terms of chemistry, symmetry and M2 bonding topology. In addition, new high-pressure X-ray diffraction data are reported for jadeite. Clinopyroxenes have been the subject of many recent high-pressure single-crystal X-ray diffraction studies (Hugh-Jones and Angel 1994; Hugh-Jones et al. 1997; Zhang et al. 1997; Arlt et al. 1998; Yang et al. 1999; Arlt and Angel 2000; Hattori et al. 2000; Tribaudino et al. 2000; Origlieri et al. 2003; Gatta et al. 2005; Bindi et al. 2006; Downs and Singh 2006; Nestola et al. 2006a). Many of the clinopyroxenes have been found to undergo phase transitions with pressure, changing symmetry between *C2/c* and *P2₁/c*. For example, spodumene (LiAlSi₂O₆), LiScSi₂O₆ (Arlt and Angel 2000), and LiFeSi₂O₆ (Pommier et al. 2005) transform from *C2/c* to *P2₁/c* with increasing pressure. ZnSiO₃ exhibits two transitions, from *C2/c* to *P2₁/c* and to *C2/c* with increasing pressure (Arlt and Angel 2000). Previous attempts to examine systematics of clinopyroxene compressibilities have been thwarted by these phase transitions, which cause Birch-Murnaghan fits to cell parameter data across phase transitions to

give spurious results, especially the K'_0 values. Recognition of the clinopyroxene phase transitions has allowed better calculation of compressibilities for these structures. The K'_0 values—the accuracy of which reflect the quality of the cell parameter data and indicate the goodness of the Birch-Murnaghan fit to the data—now average ~3.5 for the clinopyroxenes considered in this study (Table 1). Still, a large dispersion exists in the compressibilities of clinopyroxenes, which cannot be explained by unrecognized phase transitions or poor data quality.

Pyroxenes are a major component of the Earth's upper mantle. It appears that much of the upper mantle is composed of clinopyroxene, since orthopyroxene transforms to monoclinic symmetry at pressure equivalent to a depth of ~225 km (Hugh-Jones et al. 1996; Woodland 1998). The mantle contains non-trivial amounts of Na that may be incorporated into Na-clinopyroxenes. McDonough and Sun (1995) estimated a Na₂O content of the bulk silicate Earth (BSE) of 0.36%, equivalent to 2670 ppm Na. The major concentration mechanism for incompatible elements such as Na occurs at mid-ocean ridges, where mantle partial melting serves to partition Na into the basaltic oceanic crust. Average mid-ocean ridge basalt (MORB) contains ~2.5% Na (McKenzie and Bickle 1988), an enrichment of one order of magnitude over BSE. Most MORB is returned to the mantle via subduction, and may be carried as deep as the lower mantle as part of the subduct-

* E-mail: mccarthy@geo.arizona.edu

TABLE 1. Constrained bulk moduli and other parameters, determined by high-pressure single-crystal X-ray diffraction, for pyroxenes considered in this study

M2M1	Space group	Mineral name	Pressure range (GPa)	No. measured cell parameters	Fitted V_0^* (Å ³)	Constrained bulk modulus (GPa)*	M2-O3 bonds†	Sympathetic or Antipathetic?	Ref.
LiAl	C2/c	spodumene	0–3.19	7	388.87	147.7	2,3	anti	b
NaAl	C2/c	jadeite	0–9.17	16	402.03	134.4	2,3	anti	a
NaAl	C2/c	jadeite	0–8.31	13	402.42	135.5	2,3	anti	c
NaFe	C2/c	aegirine	0–11.55	15	428.72	117.2	2,3	anti	d
NaFe	C2/c	aegirine	0–9.74	12	429.25	117.5	2,3	anti	c
NaCr	C2/c	kosmochlor	0–9.28	19	418.87	127.5	2,3	anti	e
CaMg	C2/c	diopside	0–10.16	10	438.64	117.2	2,3, 1,4	both	g
CaMg	C2/c	diopside	0–9.97	33	438.56	112.4	2,3, 1,4	both	h
(Ca _{0.80} Mg _{0.20})(Mg _{1.00})	C2/c	diopside	0–15.1	23	436.55	118.6	2,3, 1,4	both	q
(Ca _{0.88} K _{0.12})(Mg _{0.83} Al _{0.17})	C2/c	diopside	0–9.48	16	435.52	124.1	2,3, 1,4	both	i
CaNi	C2/c	n/a	0–7.76	18	435.20	124.0	2,3, 1,4	both	n
CaFe	C2/c	hedenbergite	0–9.97	33	449.86	118.0	2,3, 1,4	both	h
ZnZn	C2/c	n/a	0–1.92	7	442.77	73.9	none	–	b
ZnZn	HP C2/c	n/a	4.90–7.43	6	423.57	90.8	14	symp	b
LiFe	P2 ₁ /c	n/a	1.08–7.22	16	414.82	94.0	2	symp	j
(Li _{0.85} Mg _{0.05} Fe _{0.06})(Fe _{0.85} Mg _{0.15})	P2 ₁ /c	n/a	0–6.83	17	415.67	96.0	2†	symp?	o
LiSc	P2 ₁ /c	n/a	0.66–4.80	9	440.39	85.1	2	symp	b
LiAl	P2 ₁ /c	spodumene	3.34–8.84	7	385.50	119.6	2 then 2,4	symp	b
ZnZn	P2 ₁ /c	n/a	1.99–4.80	9	439.63	68.8	1,3	symp	b
MgMg	Pbca	enstatite	0–8.51	26	416.25	115.8	2,4	symp	k
(Mg _{0.59} Fe _{0.41})(Mg _{0.59} Fe _{0.41})	Pbca	enstatite	0–7.50	17	424.19	113.0	2,4	symp	l
(Mg _{0.66} Fe _{0.24} Al _{0.08} Ca _{0.01})(Mg _{1.00})	Pbca	enstatite	0–8.62	21	416.44	122.6	2,4	symp	l
FeFe	Pbca	ferrosillite	0–5.41	17	437.60	109.1	2,4	both	l
(Mg _{0.93} Ca _{0.07})(Mg _{1.00})	Pbca	enstatite	0–10.16	10	419.07	118.9	2,4	symp	p
(Mg _{0.77} Sc _{0.23})(Mg _{0.77} Li _{0.23})	P2 ₁ /cn	enstatite	2.50–9.98	5	424.39	111.4	1+	?	m

Notes: Values have been recalculated using reported cell parameters from the literature. Bulk moduli vs. ambient cell volumes from this table are plotted in Figure 9. Column labels are defined as follows: M2M1 = identification of the atoms in the M2 and M1 sites. Space group = space group of the structure over the pressure range used to calculate bulk modulus. Mineral name = mineral name, if applicable. Many pyroxenes reported here do not occur naturally and thus do not have mineral names. Pressure range = the pressure range over which cell parameters were collected and used to calculate bulk modulus. No. measured cell parameters = the number of measured cell parameters fit to calculate bulk modulus. Fitted V_0 = the resulting fit V_0 from our software used to fit the P - V data. Constrained bulk modulus = bulk modulus calculated with Down's BMUR software, with $K_0^* = 4.0$. M2-O3 bonds = identity of existing M2-O3 bonds following the nomenclature of Downs (2003). Sympathetic or Antipathetic? = nature of the M2-O3 bonds in relation to Si chain kinking (see text). Ref. = References: (a) This study; (b) Arlt and Angel (2000); (c) Nestola et al. (2006a); (d) Downs and Singh (2006); (e) Origlieri et al. (2003); (g) Thompson et al. (in preparation); (h) Zhang et al. (1997); (i) Bindi et al. (2006); (j) Downs et al. (in preparation); (k) Hugh-Jones and Angel (1994); (l) Hugh-Jones et al. (1997); (m) Yang et al. (1999); (n) Nestola et al. (2005); (o) Gatta et al. (2005); (p) Nestola et al. (2006b); (q) Tribaudino et al. (2000).

* K_0^* constrained to 4.0. For comparison with clinopyroxenes, orthopyroxene cell volumes are halved.

† Numbers represent the O atoms to which M2 is bonded, following the nomenclature of Downs (2003).

ing oceanic lithosphere (van der Hilst et al. 1997). Holland (1980) defined the P - T conditions of the albite (NaAlSi₃O₈) ↔ jadeite + quartz reaction over the range 600–1200 °C and 15–35 kbar, showing that albite transforms to jadeite at conditions near the crust-mantle boundary. Gasparik (1992) calculated the high- P and high- T stability fields of the jadeite-enstatite (MgSiO₃) join, concluding that jadeite is stable up to ~20 GPa at mantle temperatures. These studies constrain the mantle stability field of jadeite from lower crust to ~600 km depth. However, at low concentrations (<5%), jadeite is a soluble component in other pyroxenes. Thus, while it is unlikely that jadeite is present as a free phase in the mantle, except in localized areas, the properties of the jadeite component of the mantle are still significant.

Pyroxenes dominated by the major mantle metals (i.e., Mg, Fe, Si, and Ca) have been the subject of extensive study at high pressures and at high temperatures, as tabulated in Yang and Prewitt (2000). A primary motivation of much of the high- P and high- T work was to identify phase transitions in these pyroxenes, which, if they occur in the mantle, could result in discontinuities in mantle properties (cf. Gasparik 1989; Duffy et al. 1995; Hugh-Jones et al. 1996).

Less common pyroxenes such as Na-dominated clinopyroxenes have not been studied as much at P , although some data exist. In a recent study of the compressibilities of jadeite and aegirine, Nestola et al. (2006a) determined cell parameters as a

function of pressure, and examined changes in compressional anisotropy with variations in chemistry along the jadeite-aegirine (NaFeSi₂O₆) solid solution. However, no structural data were determined in their study. Zhao et al. (1997) performed a synchrotron X-ray powder diffraction study on jadeite at simultaneous P and T to 8.2 GPa and 1280 K. They fit their data with a modified Birch-Murnaghan equation of state, with $K_0^* = 5.0$, and found the bulk modulus of jadeite to be 125(4) GPa. Cameron et al. (1973) examined the jadeite structure at four temperatures from ambient to 800 °C. They found that jadeite cell parameters (a , b , c , β) and average M-O distances (Na-O, Al-O) increased linearly with temperature. No significant changes in Si-O bond lengths were observed, although rotation of the SiO₄ tetrahedra, on the order of a few degrees, was found to accommodate some of the expansion of the structure.

The pyroxene structure consists of chains of edge-sharing M1 octahedra and chains of corner-linked Si tetrahedra, both parallel to c . Large, irregular M2 polyhedra reside between, and cross-link, the M1 and T chains. It has been suggested that compressibility of C2/c pyroxenes seems to be controlled, to a first order, by the M1O₆ chains. Size of the M1 cation is positively correlated with ambient unit-cell volumes (Thompson and Downs 2004). The same authors demonstrate that M2 cation size is not correlated with unit-cell volume. The tetrahedral chain links are relatively flexible and the chain length can vary along c

by tetrahedral rotation, associated with change in the O3-O3-O3 angle and Si-Si distances. The tetrahedra themselves compress very little due to the short O-O contacts related to the strong, short Si-O bonds. Average O-O polyhedral edge lengths in jadeite at ambient pressure are as follows: NaO₆, 2.90 Å; AlO₆, 2.72 Å; SiO₄, 2.65 Å. Atoms at M2 in clinopyroxenes reside in a site with irregular coordination that varies from four- to eightfold, depending on the structure. The M2-O bonds tend to be long and compressible compared to M1-O bonds. Thus M2 was not thought to have much effect on pyroxene compression. Downs (2003) indicates that the only variation in bonding topology of the pyroxenes involves M2-O3 bonds, where O3 are bridging O atoms in the tetrahedra chains. An examination of C2/c pyroxenes indicates that coordination of M2 cations appears to be correlated with the charge of the cation.

In this study, we consider the details of M2 bonding, specifically how M2-O3 bonds relate geometrically to SiO₄ rotations induced by increasing pressure. We find that the relationship of M2-O3 bonding with SiO₄ rotation is one factor controlling clinopyroxene compressibilities, although the characteristics of the M1 polyhedra do exert the primary control. Three types of M2-O3 relationships are postulated, and two are observed in this study.

EXPERIMENTAL METHODS

A natural jadeite crystal from Clear Creek, San Benito County, California, U.S.A., supplied by Hatt Yoder, was selected for study based on crystal quality as determined by examination of peak profiles. A crystal from the same sample was used by Prewitt and Burnham (1966) in their original description of the jadeite structure. Typical peak widths were 0.10° in \square . The size of the crystal was 80 × 70 × 40 μm . The composition of a jadeite crystal picked from the same hand specimen was determined by an average of 20 microprobe analyses to be Na_{1.002(8)}Al_{1.000(10)}[Si_{1.979(8)}Al_{0.024(2)}]_{22.003(8)}O₆. The same piece, numbered R050220, was examined as part of the RRUFF project, and information on these analyses can be found at www.ruff.info.

Diffraction data were collected with an automated Picker four-circle diffractometer using unfiltered MoK α radiation and operating at 45 kV and 40 mA. Before loading in the diamond cell, the crystal was examined in air. The positions of 28 high-intensity peaks ($9^\circ < 2\theta < 33^\circ$) were determined using a modification of the eight-peak centering technique of King and Finger (1979), by fitting both K α_1 and K α_2 profiles with Gaussian functions. Refined cell parameters constrained to monoclinic symmetry are given in Table 2. A half sphere of intensity data were collected to $2\theta \leq 60^\circ$, using ω scans of 1° width, step size 0.025° , and 5 s per step counting times. The structure was refined on F with anisotropic displacement parameters using a modification of RFINE (Finger and Prince 1975) to $R_w =$

0.027. Structural data at room conditions are summarized in Table 3. These data have smaller errors than Prewitt and Burnham (1966) ($R = 0.040$), but otherwise compare favorably.

The jadeite crystal was loaded into a four-pin Merrill-Bassett type diamond-anvil cell with beryllium seats. The vector perpendicular to the (110) plane was oriented parallel to the diamond-anvil cell axis. The diamond anvil culet size was 600 μm . A 250 μm thick stainless steel gasket, pre-indented to 120 μm , with a hole diameter of 350 μm , was used. Along with the jadeite crystal, the cell was loaded with a small ruby fragment and a 4:1 mixture of methanol:ethanol as pressure medium. Ruby fluorescence spectra were collected before and after each collection of intensity data, and the positions of the R_1 and R_2 peaks were determined by fitting with Lorentzian functions. Pressure was calculated from the fitted R_1 and R_2 peak positions using the function of Mao et al. (1978), with an estimated error of ± 0.05 GPa.

The experiment was carried out to a pressure of 9.17 GPa. The gasket failed when the pressure was raised further. Unit-cell data were collected at 16 pressures, and intensity data were collected at 9 of these pressures. Every accessible reflection allowed by C2/c symmetry, up to 672 intensity data ($2\theta \leq 60^\circ$), were collected at pressure, with ω scans of 1° width, in steps of 0.025° and counting times of 10 s per step. These data reduced to 214 symmetry-equivalent reflections. Reflections violating C2/c were examined, but none with significant intensities were found throughout the experiment. Absorption corrections for the beryllium seats and diamond anvils were made from an absorption correction profile of the empty diamond cell. Structure factors were weighted by $\omega = [\sigma_F^2 + (pF)^2]^{-1}$, where σ_F was obtained from counting statistics and p chosen to ensure normally distributed errors (Ibers and Hamilton 1974). Structural data were refined with isotropic displacement factors using a modified version of RFINE (Finger and Prince 1975) and are summarized in Table 4. R_w ranged from 0.027 to 0.047.

Bond lengths and angles were calculated using BOND91 software, modified after Finger and Prince (1975). Polyhedral volumes and quadratic elongations were obtained with XTALDRAW (Downs and Hall-Wallace 2003). Selected bond lengths, angles, and polyhedral volumes are presented in Table 5.

RESULTS AND DISCUSSION

A third-order Birch-Murnaghan equation was fit to the data in Table 2 to determine a pressure-volume equation of state for jadeite, resulting in $V_0 = 402.03(2) \text{ \AA}^3$, $K_0 = 137(1) \text{ GPa}$, and $K'_0 = 3.4(4)$, or $V_0 = 402.03(2) \text{ \AA}^3$ and $K'_0 = 134.4(3) \text{ GPa}$ with $K'_0 \equiv 4.0$. Our values closely match those reported by Nestola et al. (2006a): $V_0 = 402.26(2) \text{ \AA}^3$, $K_0 = 134.0(7) \text{ GPa}$ and $K'_0 = 3.7(6)$. Brillouin spectroscopy has also been used to determine single-crystal elasticity of jadeite from the same locality, with results ($K_0 = 143 \text{ GPa}$) similar to those from this study (Kandelin and Weidner 1988). Constraining K_0 to the value derived from Brillouin measurements (143 GPa) results in $V_0 = 402.01(2)$ and $K'_0 = 1.6(1)$. Our data and fitted curve are plotted in Figure 1. The compressibility of jadeite, reflected by V/V_0 , is compared to other Na clinopyroxenes in Figure 2. No evidence of a phase transition in jadeite was observed to a pressure of 9.17 GPa. All observed cell parameters decrease continuously with increasing pressure. Cell-parameter data were used to construct unit strain ellipsoids with STRAIN, modified after Ohashi (1982). The unit strain ellipsoid is highly anisotropic, with axial ratios of 1.00:1.63:2.10 in the range 0–9.17 GPa, and is illustrated in Figure 3. The axial values of the unit strain ellipsoid are: ϵ_1 , -0.001391 ; ϵ_2 , -0.002274 ; and ϵ_3 , $-0.002922 \text{ GPa}^{-1}$. The ϵ_3 axis is 53.7° from \mathbf{c} , and in the clinopyroxene structures, ϵ_2 is constrained to be parallel to \mathbf{b} . Our results compare well with Nestola et al. (2006a) who report unit strain ellipsoid axial ratios of 1.00:1.60:2.10 in the range 0–5.82 GPa.

Procrystal electron density analysis of jadeite indicates six Na-O bonds at room conditions (Downs 2003). Sodium in jadeite resides on a twofold symmetry axis, constraining the coordination of Na to an even number, and resulting in three

TABLE 2. Jadeite unit-cell data as a function of pressure

P (GPa)	a (Å)	b (Å)	c (Å)	β (°)	V (Å ³)
0.0001*	9.4242(2)	8.5657(2)	5.2242(2)	107.578(2)	402.03(2)
2.07*	9.3718(3)	8.5240(6)	5.1985(3)	107.399(3)	396.28(4)
3.40*	9.3372(3)	8.4966(6)	5.1805(3)	107.285(3)	392.43(4)
4.01	9.3260(5)	8.4854(9)	5.1735(4)	107.228(5)	391.04(5)
4.53	9.3112(2)	8.4724(5)	5.1656(2)	107.194(2)	389.29(3)
4.92*	9.3030(4)	8.4666(8)	5.1609(4)	107.140(4)	388.44(5)
5.22	9.2968(2)	8.4602(4)	5.1576(2)	107.124(2)	387.67(3)
5.51	9.2926(5)	8.4566(9)	5.1553(5)	107.110(5)	387.19(6)
6.1	9.2800(2)	8.4452(5)	5.1474(2)	107.056(2)	385.67(3)
6.12*	9.2793(3)	8.4446(6)	5.1474(3)	107.054(3)	385.61(4)
6.66	9.2688(4)	8.4346(8)	5.1411(4)	107.002(4)	384.36(5)
7.17*	9.2593(2)	8.4268(5)	5.1354(3)	106.979(3)	383.23(3)
7.43	9.2532(1)	8.4199(3)	5.1315(1)	106.955(1)	382.43(2)
7.83*	9.2455(4)	8.4137(8)	5.1269(4)	106.910(4)	381.57(5)
8.54*	9.2305(2)	8.3999(5)	5.1178(2)	106.854(3)	379.77(3)
9.17*	9.2185(2)	8.3871(5)	5.1099(2)	106.794(2)	378.23(3)

Note: Space group = C2/c.

* Intensity data collected at this pressure.

TABLE 3. Structural parameters for jadeite in air at room conditions

Atom	x	y	z	B_{eq} (Å ²)	β_{11}	β_{22}	β_{33}	β_{12}	β_{13}	β_{23}
NaM2	0	0.3006(1)	¼	1.305(17)	0.00432(10)	0.00419(12)	0.01090(33)	0	0.00034(15)	0
AlM1	0	0.90601(7)	¼	0.746(14)	0.00197(7)	0.00324(9)	0.00637(24)	0	0.00091(103)	0
Si	0.29063(4)	0.09334(4)	0.22786(8)	0.733(12)	0.00189(5)	0.00320(7)	0.00640(17)	-0.00007(3)	0.00094(7)	-0.00005(6)
O1	0.1093(1)	0.0759(1)	0.1280(2)	0.824(19)	0.00207(12)	0.00373(13)	0.00692(37)	-0.00006(9)	0.00093(16)	0.00014(17)
O2	0.3611(1)	0.2634(1)	0.2929(2)	0.975(19)	0.00284(11)	0.00374(13)	0.00929(36)	-0.00037(10)	0.00164(17)	-0.00031(17)
O3	0.3537(1)	0.0071(1)	0.0057(2)	0.935(19)	0.00249(10)	0.00415(129)	0.00779(19)	0.00003(12)	0.00124(14)	-0.00063(37)

Note: Space group = C2/c.

TABLE 4. Structural parameters for jadeite as a function of pressure

P (GPa)	2.07	3.40	4.92	6.12	7.17	7.83	8.54	9.17
obs refl.	229	223	218	231	226	236	184	184
total refl.	279	280	277	276	275	283	270	268
p^*	0.025	0.03	0.035	0.03	0.03	0.03	0.022	0.022
R_w	0.039	0.043	0.047	0.044	0.044	0.045	0.035	0.034
Al y	0.9066(3)	0.9072(4)	0.9077(4)	0.9076(4)	0.9081(4)	0.9075(4)	0.9080(5)	0.9078(5)
B	0.65(4)	0.72(4)	0.57(4)	0.66(4)	0.63(4)	0.62(4)	0.55(4)	0.54(4)
Na y	0.3010(5)	0.3021(5)	0.3032(6)	0.3029(5)	0.3025(5)	0.3039(6)	0.3043(6)	0.3044(6)
B	1.24(5)	1.29(6)	1.12(6)	1.10(6)	1.16(6)	1.13(6)	0.92(6)	1.06(6)
Si x	0.2910(1)	0.2912(1)	0.2913(2)	0.2914(1)	0.2913(1)	0.2913(2)	0.2915(2)	0.2913(2)
y	0.0939(2)	0.0941(2)	0.0945(3)	0.0946(2)	0.0946(2)	0.0948(2)	0.0956(3)	0.0957(3)
z	0.2285(2)	0.2284(2)	0.2290(3)	0.2289(2)	0.2291(3)	0.2291(3)	0.2297(3)	0.2297(3)
B	0.63(3)	0.67(3)	0.61(4)	0.65(3)	0.64(3)	0.65(3)	0.51(3)	0.55(3)
O1 x	0.1089(3)	0.1085(3)	0.1081(4)	0.1086(3)	0.1086(3)	0.1085(3)	0.1082(4)	0.1087(4)
y	0.0780(5)	0.0788(5)	0.0787(6)	0.0787(6)	0.0779(6)	0.0789(6)	0.0801(7)	0.0799(7)
z	0.1286(6)	0.1288(6)	0.1288(7)	0.1294(6)	0.1295(7)	0.1293(7)	0.1295(7)	0.1306(7)
B	0.63(6)	0.74(6)	0.63(7)	0.65(6)	0.74(6)	0.59(6)	0.58(7)	0.60(7)
O2 x	0.3610(3)	0.3606(4)	0.3608(4)	0.3601(4)	0.3610(4)	0.3602(4)	0.3599(4)	0.3609(4)
y	0.2639(6)	0.2650(6)	0.2664(7)	0.2658(6)	0.2675(7)	0.2672(7)	0.2672(7)	0.2677(7)
z	0.2954(6)	0.2975(6)	0.2988(7)	0.3002(6)	0.3012(6)	0.3024(6)	0.3032(7)	0.3040(7)
B	0.95(6)	0.92(7)	0.86(7)	0.87(7)	0.84(7)	0.86(7)	0.78(7)	0.95(8)
O3 x	0.3543(3)	0.3550(3)	0.3554(4)	0.3562(3)	0.3562(4)	0.3570(4)	0.3570(4)	0.3573(4)
y	0.0099(6)	0.0087(7)	0.0111(8)	0.0128(7)	0.0138(7)	0.0148(7)	0.0142(8)	0.0145(9)
z	0.0048(5)	0.0037(6)	0.0022(7)	0.0018(6)	0.0005(6)	0.0016(6)	0.0005(7)	-0.0005(8)
B	0.76(6)	0.88(6)	0.78(7)	0.81(6)	0.86(6)	0.73(6)	0.63(7)	0.78(7)

Note: $x_{Al} = x_{Na} = 0$; $z_{Al} = z_{Na} = ¼$.* Weights computed by $\omega = [\sigma_F^2 + (pF)^2]^{-1}$.**TABLE 5.** Selected bond lengths (Å), volumes (Å³), distortion parameters, and angles (°) from structure refinements

P (GPa)	0.0001§	2.07	3.40	4.92	6.12	7.17	7.83	8.54	9.17
R(SiO1)	1.636(1)	1.634(3)	1.634(3)	1.634(4)	1.628(3)	1.624(3)	1.623(3)	1.625(3)	1.617(3)
R(SiO2)	1.595(1)	1.586(5)	1.587(5)	1.591(6)	1.580(5)	1.593(5)	1.585(5)	1.575(6)	1.580(6)
R(SiO3a)	1.632(1)	1.621(4)	1.627(4)	1.624(4)	1.618(4)	1.617(4)	1.611(4)	1.618(4)	1.622(5)
R(SiO3b)	1.637(1)	1.640(4)	1.627(4)	1.627(5)	1.631(5)	1.627(4)	1.636(5)	1.628(5)	1.624(6)
<R(SiO)>	1.6247	1.6203	1.6189	1.6187	1.6140	1.6147	1.6136	1.6116	1.6109
V(SiO ₄)	2.1833	2.1678	2.1621	2.1619	2.1436	2.1481	2.1424	2.1342	2.1304
TAV*	22.9813	20.2149	19.6380	19.1417	18.7610	19.6542	18.6671	18.6510	20.2520
MTQE†	1.0055	1.0049	1.0048	1.0047	1.0045	1.0047	1.0045	1.0045	1.0048
R(NaO1)	2.360(1)	2.332(5)	2.324(6)	2.321(6)	2.313(6)	2.311(6)	2.310(6)	2.299(7)	2.297(7)
R(NaO2)	2.414(1)	2.397(3)	2.388(3)	2.381(4)	2.371(3)	2.363(4)	2.360(4)	2.356(4)	2.348(4)
R(NaO3c)	2.366(1)	2.371(5)	2.349(6)	2.352(7)	2.357(6)	2.364(6)	2.354(6)	2.346(7)	2.345(7)
R(NaO3d)	2.741(1)	2.702(5)	2.683(5)	2.647(6)	2.627(5)	2.613(5)	2.595(5)	2.587(5)	2.576(6)
diff‡	0.375	0.331	0.334	0.295	0.270	0.249	0.241	0.241	0.231
<R(NaO)>	2.470	2.451	2.436	2.425	2.417	2.413	2.405	2.397	2.392
R(AlO1a)	1.996(1)	1.990(4)	1.981(5)	1.966(5)	1.964(4)	1.951(4)	1.957(4)	1.956(5)	1.952(5)
R(AlO1b)	1.938(1)	1.932(3)	1.926(3)	1.920(3)	1.920(3)	1.918(3)	1.915(3)	1.912(3)	1.916(4)
R(AlO2)	1.853(1)	1.848(5)	1.845(5)	1.834(5)	1.839(5)	1.823(5)	1.827(5)	1.830(6)	1.819(6)
<R(AlO)>	1.9288	1.9233	1.9175	1.9072	1.9078	1.8996	1.8996	1.8956	1.8956
V(AlO ₄)	9.3676	9.2955	9.2119	9.0623	9.0759	8.9299	8.9568	8.9511	8.9079
OAV*	47.7746	45.5977	45.5225	45.9720	44.8669	44.7608	45.5179	44.8290	43.3377
MOQE†	1.0151	1.0145	1.0144	1.0146	1.0141	1.0142	1.0144	1.0141	1.0139
Si-O3-Si	139.12(7)	138.8(2)	138.6(2)	138.2(3)	137.6(2)	137.4(2)	136.8(2)	137.0(3)	136.7(3)
O3-O3-O3	174.7(1)	172.6(5)	173.5(5)	171.7(6)	170.4(6)	169.7(5)	168.9(5)	169.4(6)	169.2(6)

* TAV/OAV = Tetrahedral/octahedral angle variance.

† MTQE/MOQE = Mean tetrahedral/octahedral quadratic elongation.

‡ diff = length difference between the shortest and longest reported Na-O bonds.

§ Structure at 0.0001 GPa was refined with anisotropic temperature factors. The O3a in SiO3a is at [0.355, 0.008, 0.004]. The O3c in NaO3c is at [0.145, 0.508, 0.496]. The O1a in AlO1a is at [0.108, 0.078, 0.129].

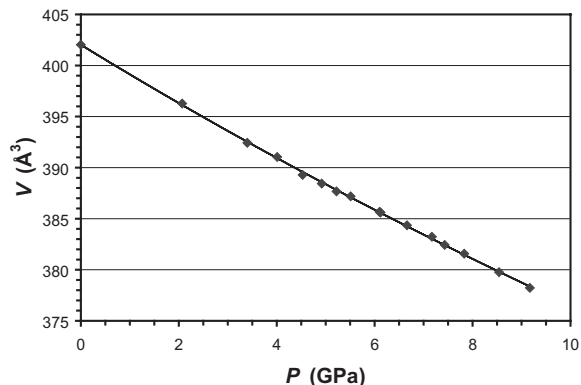


FIGURE 1. Unit-cell volume as a function of pressure for jadeite. Data are fit with a third-order Birch-Murnaghan equation, with $V_0 = 402.03(2) \text{ \AA}^3$, $K_0 = 137(1) \text{ GPa}$, and $K'_0 = 3.4(4)$. Errors in P and V are significantly smaller than the symbols used.

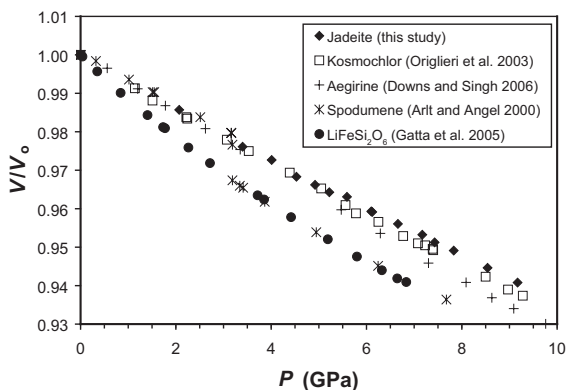


FIGURE 2. Normalized unit-cell volumes vs. pressure for jadeite, and for a selection of $C2/c$ and $P2_1/c$ pyroxenes from the literature. The jadeite unit-cell volume decreases less than that of other clinopyroxenes over the P range examined. Errors in P and V are significantly smaller than the symbols used.

pairs of equivalent Na-O bonds. In this paper, equivalent bonds are represented, for example, in the manner $\text{Na-O}_{2,3}$, where Na is bonded to O_{3_2} and O_{3_3} , which are symmetrically equivalent atoms. Figure 4b shows the environment around Na in jadeite, which is bonded to two O_1 , two O_2 , and the two bridging O atoms O_{3_2} and O_{3_3} , following the nomenclature of Downs (2003). The nearest unbonded O atoms are O_{3_1} and O_{3_4} , at a distance of $2.741(1) \text{ \AA}$ from Na at ambient pressure. All Na-O distances in jadeite decrease with pressure, although at different rates (Fig. 5). The $\text{Na-O}_{3_{1,4}}$ distance decreases at nearly 10 times the rate of the $\text{Na-O}_{2,3}$ distance, the bond distance displaying the least decrease with pressure. Linear extrapolation of the decreasing $\text{Na-O}_{2,3}$ and $\text{Na-O}_{3_{1,4}}$ distances shows they would be the same length at 22.8 GPa . At this or a lesser pressure, jadeite is expected to undergo a bonding transition as Na forms bonds to $\text{O}_{3_{1,4}}$. The longest Na-O bond in jadeite at room conditions is $\text{Na-O}_{3_{2,3}}$, at $2.414(1) \text{ \AA}$. It may be more reasonable to assume $\text{Na-O}_{3_{1,4}}$ bond formation at this Na-O distance rather than the extrapolated, decreasing $\text{Na-O}_{2,3}$ distance. In this case, the linearly extrapolated

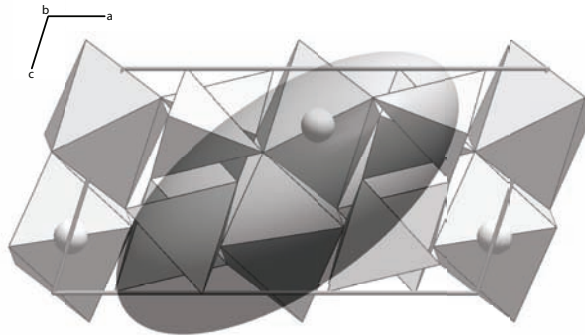


FIGURE 3. Oriented unit strain ellipsoid superimposed on the jadeite structure viewed down b . M2 (Na) is illustrated as a sphere. Although edge-sharing M1O_6 polyhedral chains are thought to control compressibility of pyroxene structures, the most compressible direction in jadeite is only $\sim 54^\circ$ from c .

$\text{Na-O}_{3_{1,4}}$ distance reaches 2.414 \AA at a pressure of 17.8 GPa .

The Al atom in jadeite resides in the octahedral M1 site. It is 6-coordinated with oxygen at all pressures in this study. Al-O bond lengths decrease systematically with pressure (Fig. 6). The Al octahedron becomes more regular with pressure, with the mean quadratic elongation decreasing from 1.0151 at ambient conditions to 1.0139 at 9.17 GPa .

The $\angle \text{O}_3\text{-O}_3\text{-O}_3$ in jadeite decreases from $174.7(1)^\circ$ at ambient conditions to $169.2(6)^\circ$ at 9.17 GPa (Fig. 7). The decrease is approximately linear with pressure and the slope is similar to that found for kosmochlor ($\text{NaCrSi}_2\text{O}_6$) (Origlieri et al. 2003). In both minerals, the silicate tetrahedra become more O-rotated with increased pressure. Ideal pyroxenes with perfectly closest-packed oxygen arrays exhibit $\text{O}_3\text{-O}_3\text{-O}_3$ angles of 120° (cubic) and 240° (hexagonal) (Thompson 1970). Thus the O atoms in jadeite move toward a cubic-closest-packed arrangement with pressure, but they are still far from it at 9.17 GPa . The distortion from a cubic closest-packed arrangement of O atoms is reflected by the mismatch in nearest neighbor O-O distances at the edges of the three types of polyhedral units, as described above.

The M2-O3 distances in Na-clinopyroxenes are positively correlated with unit-cell volumes as shown in Figure 8. Structures with the smallest unit-cell volumes have the shortest M2-O3 bonds. Jadeite has the smallest unit-cell volume of any Na-pyroxene in this study (Table 1), and thus has the shortest unbonded, nearest-neighbor M2-O3 distance [$\text{Na-O}_{3_{1,4}}$ distance of $2.741(1) \text{ \AA}$]. $C2/c \rightarrow C2/c$ bonding transitions may occur in $C2/c$ pyroxenes with pressure as M2-O3 bond pairs form or break. In a Raman spectroscopy study of diopside ($\text{CaMgSi}_2\text{O}_6$), Chopelas and Serghiou (2002) observed discontinuities in Raman spectra as a function of pressure. They attributed this change to $C2/c \rightarrow C2/c$ transitions, with Ca coordination changing from eight to six with increasing pressure. Origlieri et al. (2003) reported incipient M2-O3 bond formation in kosmochlor with pressure, which would represent a $C2/c \rightarrow C2/c$ transition. Still, such a transition has not been observed in a high-pressure X-ray diffraction study. The Na-pyroxene that undergoes a $C2/c \rightarrow C2/c$ transition at lowest pressure is likely to be determined by the (nearest neighbor) unbonded M2-O3 distance and the rate of decrease of this distance with pressure. Jadeite, with its short

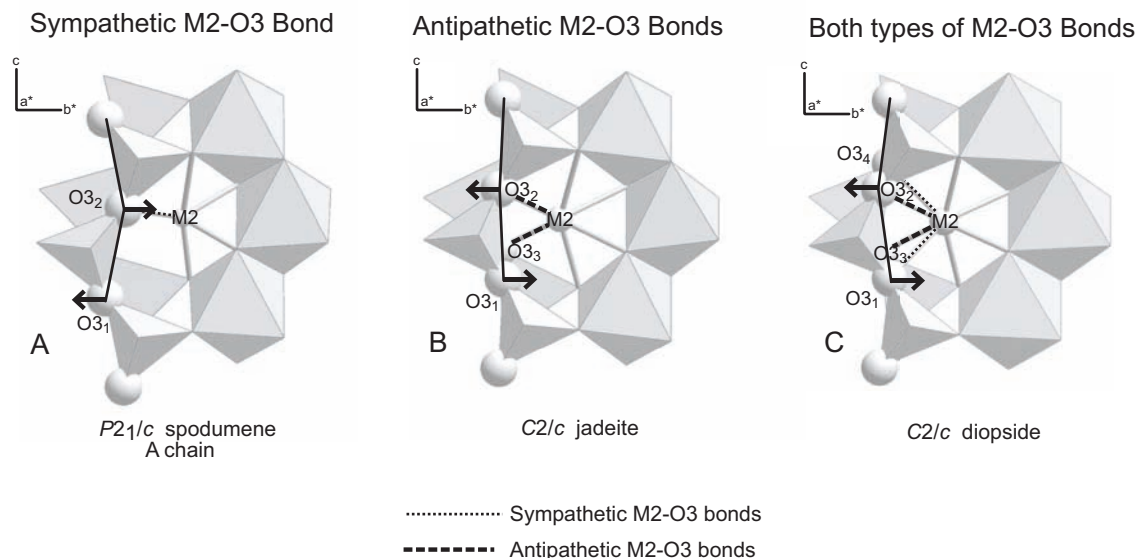


FIGURE 4. Various M2-O bonding topologies exhibited by the clinopyroxene structures examined in this study. View is down a^* . The solid lines connect the center of bridging (O3) O atoms, which are labeled following the nomenclature of Downs (2003). The arrows represent schematically the displacement direction of the O3 atoms, relative to the unit cell, as pressure increases. Although all interatomic distances in jadeite decrease with pressure, distances associated with sympathetic M2-O3 movement decrease more with pressure than suggested by a purely compressional model. (a) M2-O bonding in $P2_1/c$ spodumene, which is characteristic of all the Li- $P2_1/c$ pyroxenes in this study. M2 has one sympathetic bond with O3, and no antipathetic bonds, making the structure more compressible than jadeite- or diopside-type structures. (b) M2-O bonding in jadeite, which is characteristic of all the $M2^{1+}$ $C2/c$ pyroxenes in this study. M2 has two antipathetic bonds to O3, which makes this structure stiff compared to topologies lacking antipathetic bonds. (c) M2-O bonding in diopside, which is characteristic of all the Ca- $C2/c$ pyroxenes in this study. M2 has two antipathetic and two sympathetic M2-O3 bonds. Structures with this bonding topology lay on-trend with jadeite-type structures in Figure 9a, providing evidence that sympathetic M2-O3 bonds do not affect compressibilities.

unbonded M2-O3 distance, is thus a good candidate for the Na-pyroxene with the lowest $C2/c \rightarrow C2/c$ transition pressure. However, our current experiment did not reach the requisite pressure of ~ 20 GPa.

Thompson and Downs (2003) suggested that M2-T repulsion may influence distortion of pyroxene structures with pressure, specifically silicate chain bending. The M2-T distances are the shortest cation-cation distances in the jadeite structure, and decrease with pressure. Based on this short distance, the strongest cation-cation Coulomb repulsion in the jadeite structure is between the cation at M2 and the nearest Si atom (Table 6). As jadeite is compressed, the Na-O_{3,4} distance decreases dramatically (as mentioned, Fig. 5). However, the repulsion between Na and the nearest Si atom [2.985(1) Å away at ambient conditions] resists shortening of the M2-T distance.

Compressibility systematics of $C2/c$ and $P2_1/c$ pyroxenes

One goal in the study of pyroxenes is to find a model that will provide a prediction of bulk moduli. Thompson and Downs (2004) developed a model that could predict $C2/c$ pyroxene unit-cell volumes at P and T . Their model was based on the chemistry of the pyroxene and used empirically determined polyhedral expansion and contraction coefficients. Their study showed that unit-cell volume is largely a function of M1, and the bulk modulus of $C2/c$ pyroxenes depends primarily on the occupancy of the M1 site.

Another approach to predicting bulk moduli is based on the

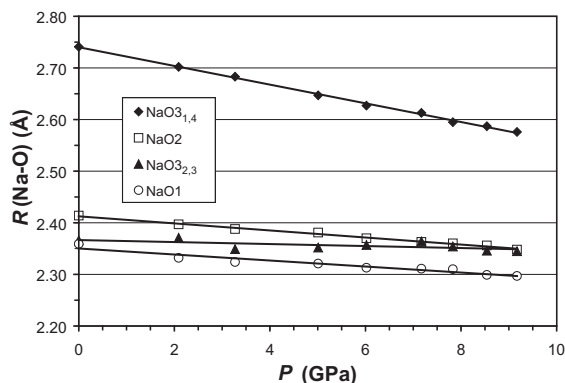


FIGURE 5. Variation of Na-O distances in jadeite with pressure at room temperature. Na-O_{3,4} is the only unbonded pair over the pressure range examined in this study. At a pressure of 17.8 GPa, the linearly extrapolated Na-O_{3,4} distance is the same as the Na-O_{3,2,3} distance at ambient pressure. At near this pressure, Na-O_{3,4} bonds may form, making Na 8-coordinated and constituting a $C2/c \rightarrow C2/c$ bonding transition. Solid lines are linear fits to the data.

observation, first made by Bridgman (1923), of the empirical relationship between bulk moduli and molar volumes of isostructural materials. Bridgman's ideas have been successfully applied by Anderson and others to a variety of minerals (cf. Anderson and Anderson 1970; Anderson 1972), as tabulated in Hazen and Finger (1982). "Bridgman's Law" implies that,

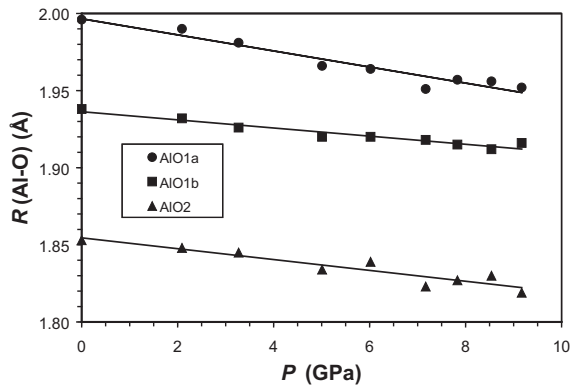


FIGURE 6. Variation of Al-O distances in jadeite with pressure at room temperature. Solid lines are linear fits to the data.

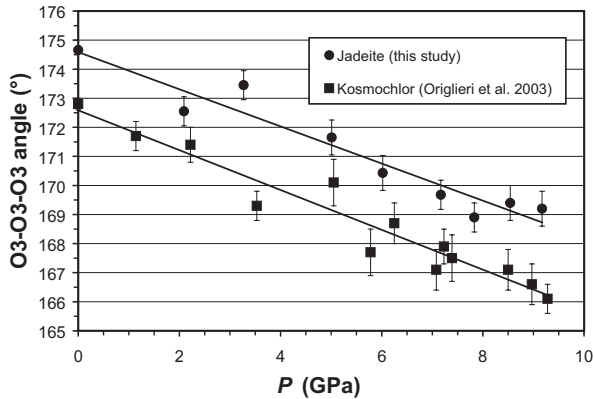


FIGURE 7. Variation of \angle O3-O3-O3 in two Na-clinopyroxenes (jadeite and kosmochlor) with pressure at room temperature. Kosmochlor data from Origlieri et al. (2003). Estimated errors in P are significantly smaller than the symbols used.

for isostructural materials, cell volumes at ambient conditions are inversely correlated with the bulk modulus. “Bridgman’s Law” seems to hold when the compressibility of a mineral is controlled by (1) shortening of cation-anion bonds as in simple oxides and halides, and/or (2) angle bending, which occurs in more topologically complex minerals such as pyroxenes, feldspars, and silica polymorphs. Angle-bending behavior is sometimes modified by bonds to bridging anions. Downs et al. (1999) examined the compressibilities of various feldspars and found them to be controlled by (1) the stiffness of T-O-T angles, which varies depending on the identity of the tetrahedral cations (e.g., Si^{4+} , Al^{3+} , B^{3+}), and (2) the number and strength of bonds between the M cations and the O atoms. Although the Al-O-Si angles found in common feldspars are roughly twice as soft as Si-O-Si angles, feldspars are generally stiffer than low-density SiO_2 polymorphs, illustrating the role of metal bonds to bridging O atoms in stiffening the feldspar structures. Among feldspars with the relatively soft Al-O-Si angles, Downs et al. (1999) proposed that microcline had a higher bulk modulus than low albite due to stiffening of the T-O-T angle by additional M-O bonds to the bridging O atoms. This is an example of an exception to

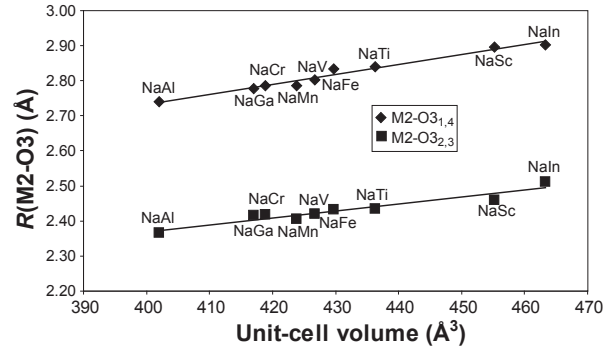


FIGURE 8. Unbonded nearest-neighbor M2-O3_{1,4} distances and bonded M2-O3_{2,3} in Na-clinopyroxenes from the literature. M2-O3_{1,4} distance is correlated with unit-cell volume at ambient conditions. Therefore, at room conditions, jadeite is the Na-clinopyroxene structure geometrically closest to a postulated $C2/c \rightarrow C2/c$ transition. Which pyroxene transforms first will also be a function of the rate of decrease in the M2-O3_{1,4} distance with P . The linear fits to the upper and lower trends have R^2 values of 0.97 and 0.91, respectively. Structural data taken from: jadeite, this study; namansilite ($\text{NaMnSi}_2\text{O}_6$), Ohashi et al. 1987; aegirine, Redhammer et al. 2000; $\text{NaTiSi}_2\text{O}_6$, Redhammer et al. 2003; jervisite ($\text{NaScSi}_2\text{O}_6$), Ohashi et al. 1994a; natilyte (NaVSi_2O_6), Ohashi et al. 1994b; kosmochlor, Origlieri et al. 2003; $\text{NaGaSi}_2\text{O}_6$, Ohashi et al. 1995; $\text{NaInSi}_2\text{O}_6$, Ohashi et al. 1990.

TABLE 6. Coulomb repulsion for selected cation-cation distances in jadeite over the pressure range in this study

P (GPa)	Repulsion (N) ($\times 10^{-28}$)					
	M2-T (edge sharing)	M2-T (2nd closest)	M1-M1	M1-M2	M1-T	T-T
0.0001	1.036	0.918	0.981	0.927	0.961	0.984
2.09	1.047	0.927	0.993	0.934	0.965	0.990
3.27	1.055	0.938	1.003	0.935	0.968	0.996
5.01	1.064	0.947	1.014	0.937	0.971	1.001
6.02	1.068	0.951	1.019	0.943	0.974	1.005
7.17	1.071	0.953	1.026	0.947	0.976	1.011
7.83	1.075	0.961	1.026	0.948	0.978	1.013
8.54	1.082	0.963	1.033	0.949	0.978	1.011
9.17	1.084	0.965	1.035	0.952	0.980	1.014

“Bridgman’s Law” since albite has a smaller unit-cell volume and thus was expected to be stiffer. Generally, then, where exceptions to “Bridgman’s Law” are observed among nearly isostructural materials, factors that modify simple bond compression and bending behavior are likely to be present.

To explore the application of “Bridgman’s Law” to the clinopyroxenes, we tabulated data from high-pressure X-ray diffraction studies in the literature (Table 1). Figure 9a is a plot of bulk moduli vs. ambient unit-cell volumes for all of the $C2/c$ and $P2_1/c$ silicate pyroxenes that we could find data for in the literature along with data from work in our lab. To create an internally consistent set of pyroxene bulk moduli, published P - V data for each pyroxene were fit with a third-order Birch-Murnaghan equation of state with K'_0 fixed at 4.0. Nestola et al. (2005) argued that fixing $K'_0 \equiv 4.0$ may be unreasonable because of the observed large range in K'_0 values for pyroxenes. However, K'_0 is so dependent on quality and number of the cell parameter data, it is likely that the unconstrained K'_0 values from the tabulated data set are unreasonable. Furthermore, we found the average unconstrained K'_0 value for $C2/c$ pyroxenes in this study to be

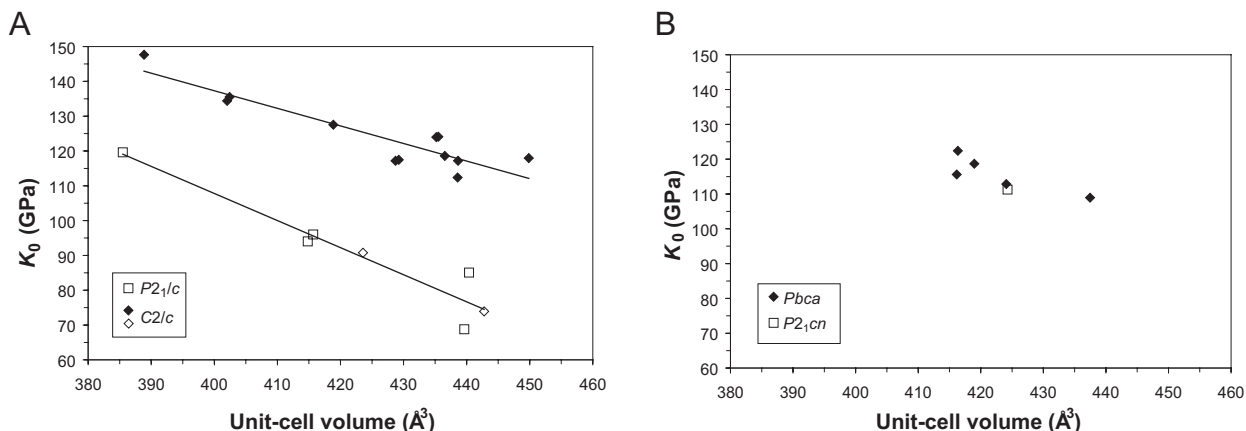


FIGURE 9. (a) Bulk moduli vs. cell volume for $C2/c$ and $P2_1/c$ silicate pyroxenes recalculated (with $K'_0 \equiv 4.0$) using data from the literature. All pyroxenes in the upper trend have two antipathetic M2-O3 bonds. Pyroxenes in the lower trend do not exhibit these bonds. The difference in M2-O3 bonding is the only topological difference among the pyroxenes considered. (b) Constrained bulk moduli vs. cell volume for $Pbca$ and $P2_1cn$ silicate pyroxenes from the literature. No clear trends are observed, perhaps due to the limited number of data points.

3.5, with a standard deviation of 2.7.

Data presented in Figure 9a show a broad vertical dispersion in K_0 of about 40 GPa with K_0 varying inversely with cell volume. The vertical dispersion can be eliminated by observing that there are two trends that diverge with increasing pressure. These trends have been illustrated by fitted lines. On first inspection, the upper trend appears to be populated by $C2/c$ pyroxenes and the lower trend by $P2_1/c$ pyroxenes. However, two $ZnSiO_3$ $C2/c$ polymorphs are exceptions, and appear to be associated with the lower trend. Based on their unit-cell volumes, the HT $C2/c$ and HP $C2/c$ $ZnSiO_3$ pyroxenes have bulk moduli much lower than expected if the upper trend were to represent $C2/c$ polymorphs. Linear fits to the upper and lower trends in the pyroxene data result in R^2 values of 0.83 and 0.91, respectively.

There is another way to distinguish these two trends, not based on symmetry, but based on bonding topology. The only significant topological difference in bonding among pyroxenes involves M2-O3 bonding, as discussed by Downs (2003). M2-O3 bonds display one of two behaviors as pyroxene structures are compressed and SiO_4 tetrahedra rotate, changing the O3-O3-O3 angles and decreasing M2-O3 distances. M2-O3 bonds whose length decreases are inhibited by pressure-induced tetrahedral rotation, which tend to resist the rotation, and are thus termed “antipathetic” bonds. In contrast, M2-O3 bonds that are further shortened by tetrahedral rotation would either assist or have no effect on tetrahedral rotation, and are thus termed “sympathetic” bonds. Both types are illustrated in Figure 4. In the $C2/c$ pyroxenes of the upper trend of Figure 9a, the M2-O_{3,4} bonds, where present, are sympathetic and the M2-O_{2,3} bonds are antipathetic. This is illustrated in Figure 5, which shows the change in Na-O distances in jadeite as a function of pressure. The antipathetic Na-O_{2,3} bonds decrease in length much more slowly than the other Na-O bonds, since tetrahedral rotation provides a component of O_{3,2,3} displacement away from Na. The Na-O_{2,3} distance has the smallest decrease with pressure while the Na-O_{3,1,4} distance has the greatest decrease. This can be interpreted as coupling of the isotropic compression of the structure (shortening all interatomic

distances) and the rotation of the silicate tetrahedra (working to shorten some interatomic distances and lengthen others). Thus *all* the structures in the upper trend are not only $C2/c$, but they have two (topologically identical) antipathetic M2-O3 bonds, adding a resistive component to compression.

In contrast, all the structures in the lower trend, regardless of symmetry, have only sympathetic M2-O3 bonds, or none at all. In particular, the HT $C2/c$ $ZnSiO_3$ has no M2-O3 bonds, while the HP $C2/c$ $ZnSiO_3$ structure has sympathetic M2-O_{3,4} bonds. Thus, the pyroxenes of the lower trend, displaying greater compressibility than the others, can be interpreted as the pyroxenes without antipathetic M2-O3 bonds. The lack of these bonds removes a component resistive to compression. Figure 4 shows three different pyroxene topologies with arrows indicating the approximate component of displacement of O3 atoms contributed by the tetrahedral rotation with compression.

It is worth noting that not all pyroxenes in the upper trend in Figure 9a have identical bonding topologies. Rather, there are two groups: (1) the monovalent-M2 $C2/c$ pyroxenes, $LiAlSi_2O_6$, $NaAlSi_2O_6$, $NaCrSi_2O_6$, and $NaFeSi_2O_6$, where M2 is 6-coordinated and bonded to two bridging O atoms, O_{3,2} and O_{3,3} (Figs. 4a and 4b), and (2) the Ca pyroxenes, $CaMgSi_2O_6$, $CaNiSi_2O_6$, and $CaFeSi_2O_6$, where Ca is 8-coordinated and bonded to all bridging O atoms, O_{3,1}, O_{3,2}, O_{3,3}, and O_{3,4} (Fig. 4b). Therefore, the upper trend in Figure 9a provides evidence that antipathetic M2-O3 bonds affect compressibility while sympathetic M2-O3 bonds do not. The monovalent-M2 $C2/c$ pyroxenes (left side of Fig. 9a) all contain two antipathetic M2-O3 bonds but no sympathetic ones. In contrast, the Ca-clinopyroxenes have two antipathetic and two sympathetic M2-O3 bonds. Still, these pyroxenes lay on-trend with the monovalent-M2 pyroxenes. If sympathetic bonds increased compressibility, the Ca-pyroxenes would be expected to lay on their own trend and to have lower bulk moduli than the monovalent-M2 $C2/c$ pyroxenes.

$P2_1/c$ pyroxene topologies vary slightly. They lack the twofold axis through M2 and thus this site is not constrained to an even number of bonds with O3 atoms. $P2_1/c$ $LiFeSi_2O_6$, $LiScSi_2O_6$, and

spodumene ($\text{LiAlSi}_2\text{O}_6$) all have identical M2 bonding topology at minimum stability pressures, with M2 bonded to one bridging oxygen, O_{3_2} , illustrated in Figure 4a. Over the pressure range 3.34–8.8 GPa, spodumene gains an M2- O_{3_4} bond (Downs 2003), making M2 6-coordinated, which gives it the same bonding topology as $P2_1/c$ ZnSiO_3 , illustrated in Figure 10.

Arlt and Angel (2000) examined the structure of ZnSiO_3 at pressures from ambient to 5.05 GPa and discovered two phase transitions over this pressure range. ZnSiO_3 is stable in space group HT $C2/c$ at room conditions, transforms to $P2_1/c$ at 1.92 GPa, and to HP $C2/c$ at ~ 4.9 GPa (Arlt and Angel 2000). It turns out that the behavior of the ZnSiO_3 polymorphs provides another confirmation of the sympathetic/antipathetic bond hypothesis. Figure 10 illustrates the three known ZnSiO_3 pyroxene structures. HT $C2/c$ ZnSiO_3 has no M2-O3 bonds. Thus this pyroxene exhibits a different topology than all other divalent-M2 $C2/c$ pyroxenes, which have topologies similar to diopside. The lack of antipathetic M2-O3 bonds appears to allow relatively unrestricted tetrahedral rotation and makes the structure the most compressible of any known $C2/c$ silicate pyroxene. The $P2_1/c$ ZnSiO_3 exhibits two M2-O3 bonds (to O_{3_2} and O_{3_4} ; see Fig. 10b). Both bonds are sympathetic to tetrahedral rotation; thus this structure is softer than $C2/c$ pyroxenes and falls on the lower trend in Figure 9a. The HP $C2/c$ ZnSiO_3 exhibits two M2-O3 bonds (to O_{3_1} and O_{3_4}); both are sympathetic.

The fact that HP $C2/c$ ZnSiO_3 is less compressible than HT $C2/c$ ZnSiO_3 provides further evidence that sympathetic M2-O3 bonds do not make pyroxene structures more compressible; rather, it appears that the important effect is that antipathetic M2-O3 bonds stiffen the structures. HP $C2/c$ ZnSiO_3 appears to be stiffer than the HT $C2/c$ polymorph due to a smaller (fitted) ambient unit cell.

An examination of the $P/V/V_0$ plot for various clinopyroxenes (Fig. 2) also shows two distinct trends. The structures of the upper trend, which include jadeite, kosmochlor, aegirine, and $C2/c$ spodumene, contain antipathetic bonds. The structures of

the lower trend do not contain antipathetic bonds. Therefore, the origin of these two trends is completely explained by our model of sympathetic and antipathetic bonding.

According to Thompson and Downs (2004), compressibility of $C2/c$ pyroxenes is controlled largely by the rigid chains of edge-sharing M1O_6 octahedra parallel to the c -axis. It seems that these chains of octahedra should resist compression because the relatively high charge of M1 cations ($2+$ or $3+$), coupled with the short M1-M1 distance, results in strong electrostatic repulsion. However, examination of the unit strain ellipsoid for jadeite show the most compressible direction is only $\sim 54^\circ$ from the axis of the M1O_6 chains ($\parallel c$). In contrast, the chains of silicate tetrahedra offer minor resistance to compression because the tetrahedra can easily rotate, as demonstrated by the decreasing O3-O3-O3 angle. Figure 7 illustrates the decrease of the O3-O3-O3 angle with pressure in jadeite and kosmochlor, the only two end-member Na clinopyroxenes that have been subjected to high-pressure X-ray diffraction structural studies.

In $C2/c$ pyroxenes, all M2-O3 distances decrease with pressure due to the decrease of all dimensions of the unit cell. To discern M2-O3 bond length changes not related solely to changes in the shape and size of the unit cell, we generated structures using the ambient atomic positions and the unit-cell parameters at each pressure at which we collected structural data. These model structures give an indication of how bond lengths would change with scaling of the unit cell but no other relative atomic translations. This approach is comparable to normalizing bond lengths to the unit-cell volume. By normalizing measured bond lengths to the bond lengths from the equivalent model structure, we can identify bond lengths that change in an unusual manner (not caused by simple cell scaling) in the real structure. Our results from jadeite and diopside are plotted in Figure 11. We observe that M2-O3 distances (bonded or unbonded) that exhibit sympathetic behavior decrease at a greater rate with pressure than expected, based on the scaled-cell model. Antipathetic M2-O3 bonds tend to become slightly longer than their model equivalents

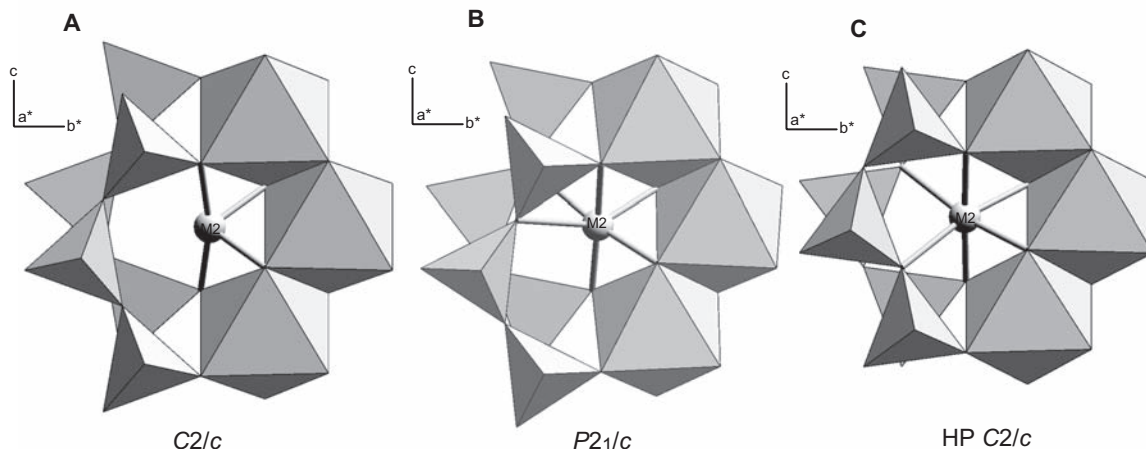


FIGURE 10. Bonding environments of the M2 cation in HT $C2/c$, $P2_1/c$, and HP $C2/c$ ZnSiO_3 structures. (a) HT $C2/c$ ZnSiO_3 , with no M2-O3 bonds, is the most compressible of all the $C2/c$ pyroxenes considered in this study ($K_0 \sim 74$ GPa). (b) $P2_1/c$ ZnSiO_3 , with two sympathetic M2-O3 bonds, is even more compressible ($K_0 \sim 69$ GPa). (c) HP $C2/c$ ZnSiO_3 , also with two sympathetic M2-O3 bonds, has a much smaller cell volume V_0 and is thus much stiffer ($K_0 \sim 91$ GPa).

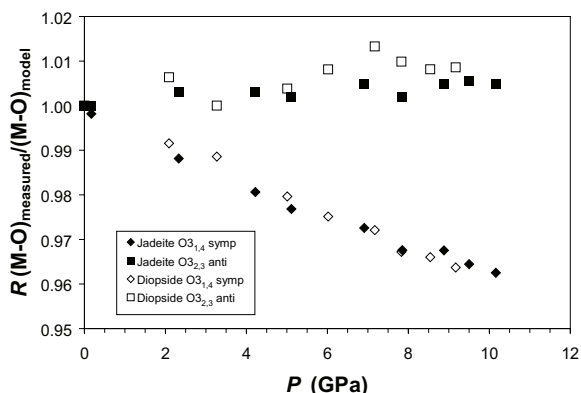


FIGURE 11. Measured M2-O3 distances normalized to model M2-O3 distances created by scaling of the unit cell and the β angle, in jadeite (solid symbols) and diopside (outlined symbols). Interatomic distances associated with sympathetic M2-O3 motion become shorter with pressure than predicted by the scaled-cell model, whereas antipathetic M2-O3 bonds become slightly longer than expected, with increasing pressure.

with pressure. This occurs because, with pressure, M2 moves toward the tetrahedral chains, but the antipathetically bonded O3 atoms move away from M2 as the tetrahedral chains kink. On the contrary, sympathetically bonded O3 atoms move toward M2 with tetrahedral chain kinking. This is, after all, what gives the bonds their sympathetic or antipathetic character.

We predict that the bulk moduli of silicate clinopyroxenes with antipathetic M2-O3 bonds should follow K_0 (GPa) = $-0.5051V_0$ (\AA^3) + 339.37 (linear fit to upper trend in Fig. 9a), whereas silicate clinopyroxenes without antipathetic M2-O3 bonds should follow K_0 (GPa) = $-0.7784V_0$ (\AA^3) + 419.14 (linear fit to lower trend in Fig. 9a). Table 7 lists predicted bulk moduli for $C2/c$ and $P2_1/c$ silicate pyroxene structures based on these equations. Structural data from high pressures are not available for many of the structures considered; therefore the antipathetic vs. sympathetic nature of the M2-O3 bonds cannot be known with certainty for these structures. However, the nature of these bonds can be estimated based on the similarity of each structure with structures known to either contain antipathetic bonds (e.g., jadeite, diopside) or to contain none (e.g., $P2_1/c$ spodumene, HP $C2/c$ ZnSiO₃). If new high-pressure structural data becomes available for any of these materials, the nature of the M2-O3 bonds can be identified and the predicted bulk modulus can be calculated based on the appropriate equation.

Where high-pressure data are not available, data at multiple temperatures may elucidate the sympathetic/antipathetic nature of M2-O3 bonds in pyroxene structures. Decreasing temperature can be analogous to increasing pressure in terms of the effect on a crystal structure of pyroxene (Hazen and Finger 1982), and increasing temperature should have the opposite effect. We suggest that the expansivities of pyroxene structures with temperature may show a dichotomy similar to that displayed by the compressibilities. Structures exhibiting only sympathetic bonds under compression would be expected to have the lower expansivities because these bonds would become resistive to the now-reversed tetrahedral rotations. However, pyroxene structures, even at temperatures approaching the melting point

TABLE 7. Predicted bulk moduli for silicate clinopyroxenes from two groups: (1) those with antipathetic M2-O3 bonds; and (2) those without such bonds

M2M1	Space group	V_0^*	Predicted K_0	Observed K_0^\dagger	Reference
Possess antipathetic M2-O3 bonds					
LiAl	$C2/c$	388.78	143.0	148(3)	b
NaAl	$C2/c$	402.03	136.3	134.4(3)	a
NaGa	$C2/c$	417.73	128.4	–	d
NaCr	$C2/c$	418.84	127.8	127.5(3)	e
NaMn	$C2/c$	423.85	125.3	–	f
NaV	$C2/c$	426.72	123.8	–	g
NaFe	$C2/c$	428.69	122.8	117(1)	h
CaNi	$C2/c$	435.21	119.5	124.0(4)	i
NaTi	$C2/c$	436.35	119.0	–	j
CaMg	$C2/c$	438.82	117.7	112.4(6)	k
CaCo	$C2/c$	443.52	115.3	–	l
CaFe	$C2/c$	449.90	112.1	118.0(4)	k
NaSc	$C2/c$	455.20	109.4	–	m
NaIn	$C2/c$	463.26	105.4	–	n
CaMn	$C2/c$	466.02	104.0	–	o

Do not possess antipathetic M2-O3 bonds

LiAl	$P2_1/c$	385.50	119.1	120(2)	b
LiCr	$C2/c$	406.10	103.0	–	c
LiGa	$C2/c$	408.30	101.3	–	c
LiV	$C2/c$	413.31	97.4	–	c
LiFe	$P2_1/c$	414.82	96.2	94(2)	p
LiFe	$C2/c$	415.78	95.5	–	c
ZnZn	HP $C2/c$	423.57	89.4	91(3)	b
LiTi	$C2/c$	423.93	89.2	–	q
ZnZn	$P2_1/c$	439.63	76.9	69(2)	b
LiSc	$C2/c$	440.21	76.5	–	b
LiSc	$P2_1/c$	440.39	76.3	85(3)	b
ZnZn	$C2/c$	442.77	74.5	74(1)	b
LiIn	$C2/c$	447.78	70.6	–	c

Notes: Measured bulk moduli from single-crystal X-ray diffraction experiments are reported where available. The sympathetic vs. antipathetic nature of M2-O3 bonds cannot be verified without structural data from several pressures (or temperatures; see text). References = (a) this study; (b) Arlt and Angel 2000; (c) Redhammer and Roth 2004; (d) Ohashi et al. 1995; (e) Origlieri et al. 2003; (f) Ohashi et al. 1987; (g) Ohashi et al. 1994b; (h) Downs and Singh 2006; (i) Nestola et al. 2005; (j) Ohashi et al. 1982; (k) Zhang et al. 1997; (l) Ghose et al. 1987; (m) Ohashi et al. 1994a; (n) Ohashi et al. 1990; (o) Freed and Peacor 1967; (p) Downs et al. in preparation; (q) Kopnin et al. 2003.

* As reported by referenced authors.

† As calculated in this study, with $K_0^* \equiv 4.0$.

of the material (i.e., ~ 1000 °C), show a small amount of expansion compared to the compression observed with pressures up to ~ 10 GPa. For example, in the classic study of the structures of several pyroxenes at high temperatures by Cameron et al. (1973), the expansion of the jadeite structure from ambient temperature to 800 °C shows an increase in the unit-cell volume of only 1.9%. In contrast, the unit-cell volume contracts by 5.9% with increased pressure over the range 0–9.17 GPa as shown in this study. Therefore, if it is even possible to elucidate antipathetic vs. sympathetic bond behavior using temperature data, the data will need to be of the highest quality.

In the proof stage of this paper it became clear that a third M2-O3 bond classification is needed. Many of the bonds we term “sympathetic” actually appear to exhibit “apathetic” behavior in the sense that they do not affect pyroxene compressibilities. True sympathetic bonds should soften their host structures. Therefore, we suggest the following nomenclature be used in future work: (1) “antipathetic” bonds stiffen host structures, (2) “sympathetic” bonds soften host structures and are not definitively observed in this study, and (3) “apathetic” bonds do not—through their relationship with tetrahedral rotation—affect the host structure’s stiffness.

Orthopyroxene compressibility

If antipathetic M2-O3 bonds resist silicate tetrahedra rotation and thus compression of clinopyroxene structures, it seems reasonable to expect a similar phenomenon in orthopyroxenes, which exhibit a similar set of M2-O3 topologies. Unfortunately, few orthopyroxenes have been subjected to high-pressure single-crystal X-ray diffraction studies to determine bulk moduli (Yang and Prewitt 2000). No clear trends are observed in the available data (Fig. 9b), except that “Bridgman’s Law” appears to hold for orthopyroxenes as well.

ACKNOWLEDGMENTS

We thank the National Science Foundation for funding our study, Compression Mechanisms of Upper Mantle Minerals, through grant no. EAR-9903104. The manuscript benefited greatly from comments by Dmitry L. Lakshtanov and an anonymous reviewer. The authors are also grateful to the late Hatt Yoder, who provided the jadeite sample used in this study.

REFERENCES CITED

- Anderson, O.L. (1972) Patterns in elastic constants of minerals important to geophysics. In E.C. Robinson, Ed., *Nature of the Solid Earth*, p 575–613. McGraw-Hill, New York.
- Anderson, D.L. and Anderson, O.L. (1970) The bulk modulus-volume relationship for oxides. *Journal of Geophysical Research*, 75, 3494–3500.
- Arlt, T. and Angel, R.J. (2000) Displacive phase transitions in C-centred clinopyroxenes: Spodumene, $\text{LiScSi}_2\text{O}_6$, and ZnSiO_3 . *Physics and Chemistry of Minerals*, 27, 719–731.
- Arlt, T., Angel, R.J., Miletich, R., Armbruster, T., and Peters, T. (1998) High-pressure $P2_1/c$ - $C2/c$ phase transitions in clinopyroxenes: Influence of cation size and electronic structure. *American Mineralogist*, 83, 1176–1181.
- Bindi, L., Downs, R.T., Harlow, G.E., Safonov, O.G., Litvin, Y.A., Perchuck, L.L., Uchida, H., and Menchetti, S. (2006) Compressibility of synthetic potassium-rich clinopyroxene: In-situ high-pressure single-crystal X-ray study. *American Mineralogist*, 91, 802–808.
- Bridgman, P.W. (1923) The compressibility of thirty metals as a function of pressure and temperature. *Proceedings of the American Academy of Arts and Sciences*, 58, 165–242.
- Cameron, M., Sueno, S., Prewitt, C.T., and Papike, J.J. (1973) High-temperature crystal chemistry of acmite, diopside, hedenbergite, jadeite, spodumene, and ureyite. *American Mineralogist*, 58, 594–618.
- Chopelas, A. and Serghiou, G. (2002) Spectroscopic evidence for pressure-induced phase transitions in diopside. *Physics and Chemistry of Minerals*, 29, 403–408.
- Downs, R.T. (2003) Topology of the pyroxenes as a function of temperature, pressure and composition determined from the procrystal electron density. *American Mineralogist*, 88, 556–566.
- Downs, R.T. and Hall-Wallace, M. (2003) The American Mineralogist crystal structure database. *American Mineralogist*, 88, 247–250.
- Downs, R.T. and Singh, A.K. (2006) Analysis of deviatoric stress from nonhydrostatic pressure on a single crystal in a diamond anvil cell: The case of monoclinic aegirine, $\text{NaFeSi}_2\text{O}_6$. *Journal of Physics and Chemistry of Solids*, 67, 1995–2000.
- Downs, R.T., Yang, H., Hazen, R.M., Finger, L.W., and Prewitt, C.T. (1999) Compressibility mechanisms of alkali feldspars: New data from reedmergnerite. *American Mineralogist*, 84, 333–340.
- Duffy, T.S., Zha, C.S., Downs, R.T., Mao, H.K., and Hemley, R.J. (1995) Elasticity of forsterite to 16 GPa and the composition of the upper mantle. *Nature*, 378, 170–173.
- Finger, L.W. and Prince, E. (1975) A system of Fortran IV computer programs for crystal structure computations. U.S. Bureau of National Standards Technical Note 854, 128 p.
- Freed, R.L. and Peacor, D.R. (1967) Refinement of the crystal structure of johannsenite. *American Mineralogist*, 52, 709–720.
- Gasparik, T. (1989) Transformation of enstatite-diopside-jadeite pyroxenes to garnet. *Contributions to Mineralogy and Petrology*, 102, 389–405.
- (1992) Enstatite-jadeite join and its role in the Earth’s mantle. *Contributions to Mineralogy and Petrology*, 111, 283–298.
- Gatta, G.D., Ballaran, T.B., and Jezi, G. (2005) High-pressure X-ray and Raman study of a ferrian magnesian spodumene. *Physics and Chemistry of Minerals*, 32, 132–139.
- Ghose, S., Wan, C., and Okamura, F.P. (1987) Crystal structures of $\text{CaNiSi}_2\text{O}_6$ and $\text{CaCoSi}_2\text{O}_6$ and some crystal-chemical relations in $C2/c$ pyroxenes. *American Mineralogist*, 72, 375–381.
- Hattori, T., Nagai, T., Yamanaka, T., Werner, S., and Schulz, H. (2000) Single-crystal X-ray diffraction of FeGeO_3 high- P clinopyroxene ($C2/c$) up to 8.2 GPa. *American Mineralogist*, 85, 1485–1491.
- Hazen, R.M. and Finger, L.W. (1982) *Comparative Crystal Chemistry: Temperature, pressure, composition and the variation of crystal structure*, 231 p. John Wiley and Sons, New York.
- Holland, T.J.B. (1980) Reaction albite = jadeite + quartz determined experimentally in the range 600–1200 °C. *American Mineralogist*, 65, 129–134.
- Hugh-Jones, D.A. and Angel, R.J. (1994) A compressional study of MgSiO_3 orthoenstatite to 8.5 GPa. *American Mineralogist*, 79, 405–410.
- Hugh-Jones, D., Sharp, T., Angel, R., and Woodland, A. (1996) The transition of orthoferrosilite to high-pressure $C2/c$ clinoferrosilite at ambient temperature. *European Journal of Mineralogy*, 8, 1337–1345.
- Hugh-Jones, D.A., Chopelas, A., and Angel, R.J. (1997) Tetrahedral compression in $(\text{Mg,Fe})\text{SiO}_3$ orthopyroxenes. *Physics and Chemistry of Minerals*, 24, 301–310.
- Ibers, J.A. and Hamilton, W.C. (1974) *International Tables for X-ray Crystallography*, IV, 366 p. Kynoch Press, Birmingham, U.K.
- Kandeljin, J. and Weidner, D.J. (1988) The single-crystal elastic properties of jadeite. *Physics of the Earth and Planetary Interiors*, 50, 251–260.
- King, H.E., Jr. and Finger, L.W. (1979) Diffracted beam crystal centering and its application to high-pressure crystallography. *Journal of Applied Crystallography*, 12, 374–378.
- Kopin, E.M., Sato, A., and Muromachi, E.T. (2003) High pressure synthesis and structure refinement of $\text{LiTiSi}_2\text{O}_6$. *Journal of Alloys and Compounds*, 354, L16–L19.
- Mao, H.K., Bell, P.M., Shaner, J.W., and Steinberg, D.J. (1978) Specific volume measurements of Cu, Mo, Pd, and Ag and calibration of the ruby R1 fluorescence pressure gauge from 0.06 to 1 Mbar. *Journal of Applied Physics*, 49, 3276–3283.
- McDonough, W.F. and Sun, S.S. (1995) The composition of the Earth. *Chemical Geology*, 120, 223–253.
- McKenzie, D. and Bickle, M.J. (1988) The volume and composition of melt generated by extension of the lithosphere. *Journal of Petrology*, 29, 625–679.
- Nestola, F., Ballaran, T.B., Tribaudino, M., and Ohashi, H. (2005) Compressional behaviour of $\text{CaNiSi}_2\text{O}_6$ clinopyroxene: Bulk modulus systematic and cation type in clinopyroxenes. *Physics and Chemistry of Minerals*, 32, 222–227.
- Nestola, F., Boffa Ballaran, T., Liebske, C., Bruno, M., and Tribaudino, M. (2006a) High-pressure behaviour along the jadeite $\text{NaAlSi}_3\text{O}_6$ -aegirine $\text{NaFeSi}_2\text{O}_6$ solid solution up to 10 GPa. *Physics and Chemistry of Minerals*, 33, 222–227.
- Nestola, F., Gatta, G.D., and Boffa Ballaran, T. (2006b) The effect of Ca substitution on the elastic and structural behavior of orthoenstatite. *American Mineralogist*, 91, 809–815.
- Ohashi, Y. (1982) A program to calculate the strain tensor from two sets of unit-cell parameters (STRAIN), p. 92–102. In R.M. Hazen and L.W. Finger, Eds., *Comparative Crystal Chemistry*. John Wiley and Sons, New York.
- Ohashi, H., Fujita, T., and Osawa, T. (1982) Crystal structure of sodium titanium silicate ($\text{NaTiSi}_2\text{O}_6$) pyroxene. *Journal of the Japanese Association of Mineralogy, Petrology and Economic Geology*, 77, 305–309.
- Ohashi, H., Osawa, T., and Tsukimura, K. (1987) Refinement of the structure of manganese sodium dimetasilicate. *Acta Crystallographica*, C43, 605–607.
- (1990) Structures of $\text{Na}(\text{In,Sc})\text{Si}_2\text{O}_6$ clinopyroxenes formed at 6 GPa pressure. *Acta Crystallographica*, B50, 838–840.
- (1994a) $\text{NaScSi}_2\text{O}_6$. *Acta Crystallographica*, B46, 742–747.
- (1994b) NaVSi_2O_6 . *Acta Crystallographica*, C50, 1652–1655.
- (1995) Low-density form of $\text{NaGaSi}_2\text{O}_6$. *Acta Crystallographica*, C51, 2476–2477.
- Origlieri, M.J., Downs, R.T., Thompson, R.M., Pommier, C.J.S., Denton, M.B., and Harlow, G.E. (2003) High-pressure crystal structure of kosmochlor, $\text{NaCrSi}_2\text{O}_6$, and systematics of anisotropic compression in pyroxenes. *American Mineralogist*, 88, 1025–1032.
- Pommier, C.J.S., Downs, R.T., Stimpfl, M., Redhammer, G.J., and Denton, M.B. (2005) Raman and X-ray investigations of $\text{LiFeSi}_2\text{O}_6$ pyroxene under pressure. *Journal of Raman Spectroscopy*, 36, 864–871.
- Prewitt, C.T. and Burnham, C.W. (1966) The crystal structure of jadeite, $\text{NaAlSi}_3\text{O}_6$. *American Mineralogist*, 51, 956–975.
- Redhammer, G.J. and Roth, G. (2004) Structural variation and crystal chemistry of $\text{LiMe}^{3+}\text{Si}_2\text{O}_6$ clinopyroxenes, $\text{Me}^{3+} = \text{Al, Ga, Cr, V, Fe, Sc}$ and In. *Zeitschrift für Kristallographie*, 219, 278–294.
- Redhammer, G.J., Amthauer, G., Lottermoser, W., and Treutmann, W. (2000) Synthesis and structural properties of clinopyroxenes of the hedenbergite $\text{CaFeSi}_2\text{O}_6$ -aegirine $\text{NaFeSi}_2\text{O}_6$ solid-solution series. *European Journal of Mineralogy*, 12, 105–120.
- Redhammer, G.J., Ohashi, H., and Roth, G. (2003) Single-crystal structure refinement of $\text{NaTiSi}_2\text{O}_6$ clinopyroxene at low temperatures ($298 < T < 100$ K). *Acta Crystallographica*, B59, 730–746.
- Thompson, J.B. (1970) Geometric possibilities for amphibole structures: model biopyriboles. *American Mineralogist*, 55, 292–293.
- Thompson, R.M. and Downs, R.T. (2003) Model pyroxenes I: Ideal pyroxene topologies. *American Mineralogist*, 88, 653–666.
- (2004) Model pyroxenes II: Structural variation as a function of tetrahedral

- rotation. *American Mineralogist*, 89, 614–628.
- Tribaudino, M., Prencipe, M., Bruno, M., and Levy, D. (2000) High-pressure behaviour of Ca-rich *C2/c* clinopyroxenes along the join diopside-enstatite ($\text{CaMgSi}_2\text{O}_6\text{-Mg}_2\text{Si}_2\text{O}_6$). *Physics and Chemistry of Minerals*, 27, 656–664.
- van der Hilst, R.D., Widiyantoro, S., and Engdahl, E.R. (1997) Evidence for deep mantle circulation from global tomography. *Nature*, 386, 578–584.
- Woodland, A.B. (1998) The orthorhombic to high-*P* monoclinic phase transition in Mg-Fe pyroxenes: Can it produce a seismic discontinuity? *Geophysical Research Letters*, 25, 1241–1244.
- Yang, H. and Prewitt, C.T. (2000) Chain and layer silicates at high temperatures and pressures. In R.M. Hazen and R.T. Downs, Eds., *High-Temperature and High-Pressure Crystal Chemistry*, 41, p. 211–255. *Reviews in Mineralogy and Geochemistry*, Mineralogical Society of America, Chantilly, Virginia.
- Yang, H., Finger, L.W., Pamela, C.G., Prewitt, C.T., and Hazen, R.T. (1999) A new pyroxene structure at high pressure: Single-crystal X-ray and Raman study of the *Pbcn-P2₁cn* phase transition in protopyroxene. *American Mineralogist*, 84, 245–256.
- Zhang, L., Ahsbahs, H., Hafner, S.S., and Kutoglu, A. (1997) Single-crystal compression and crystal structure of clinopyroxene up to 10 GPa. *American Mineralogist*, 82, 245–258.
- Zhao, Y.S., Von Dreele, R.B., Shankland, T.J., Weidner, D.J., Zhang, J.Z., Wang, Y.B., and Gasparik, T. (1997) Thermoelastic equation of state of jadeite $\text{NaAl-Si}_2\text{O}_6$: An energy-dispersive Reitveld refinement study of low symmetry and multiple phases diffraction. *Geophysical Research Letters*, 24, 5–8.

MANUSCRIPT RECEIVED NOVEMBER 27, 2006

MANUSCRIPT ACCEPTED SEPTEMBER 25, 2007

MANUSCRIPT HANDLED BY PRZEMYSŁAW DERA